The longitudinal dynamics of a road vehicle:
A new multibody approach for the equations of the rolling wheel with constraints relaxation and traction reaction saturation.

Bukoko Ikoki *

31 October 2022

Abstract

The Udwadia-Kalaba formulation is proposed to model the longitudinal dynamics of a road vehicle. To render complex situations such as spinning on a slippery road, an original approach is implemented by the relaxation of constraints in the Udwadia-Kalaba formulation for the rolling of a wheel. In a combined approach of both slip and stiction in the contact section, the constraints equations of pure rolling are associated with stiction. Such constraints are lifted as slip occurs to allow the dynamics of the wheel to take over the normally imposed kinematic contraints. The relaxation of constraints is achieved by the extension of the Udwadia-Kalaba formulation with the semi-least-squares solutions of the constraints equations. This sets biases on the constraints equations based on the description of weight functions that takes into account a friction conditionality without branching. Which leads to the smooth activation or deactivation of selected constraints equations and associated forces. Without the need to rewrite the equations of motion.

1 Introduction

In [1], Udwadia raised the unresolved problem of a proper modeling of the rolling wheel in vehicle dynamics. An attempt [2] is made in this work to address the issue. The complex wheel-and-ground interaction is modeled by considering the rolling constraint. Rolling without slipping is associated with stiction [3]. This constraint needs to be lifted as friction kicks in since a classic variational approach cannot handle dry friction. To a certain extent, the Udwadia-Kalaba formulation for non-ideal constraints [4] takes friction into consideration.

*Bukoko.Ikoki@kdynamics.ca, KDYNAMICS Logiciel, Inc. Sherbrooke, Kanada.

However, by considering the general solution of the least-squares problem associated with constraints equations, it fails to preserve the necessary minimum norm. According to Gauss' least-constraint principle, the accelerations that are found in this way are not the actual ones. As they remain bound to the constraints equations that they persistently fulfill in a least-square sense, it appears that they do not obey the dynamics of the rolling. Nevertheless, the matrix-based U-K formulation appeals in its ability to not only allow the interpretation of the physics behind the equations, conversely, it allows the transposition of an idea into equations.

In [2], we have suggested a way to relax ideal constraints whenever the additional term of non-ideal constraints comes into play in the Udwadia-Kalaba formulation. To allow the relaxation of constraints as slip occurs, the weighted semi-least-squares solutions of the constraints equations are considered instead of the non-weighted constraints equations in the classic formulation. With friction-aware weights on the constraints equations, the residuals are altered accordingly. The bias on constraints is achieved to the extent friction is important by diverting norm minimization efforts to constraints with smaller residuals. By setting the computed generalized coordinates free from selected constraints equations as needed, the true dynamics of the system is allowed to take place.

In their presentation of the joints modeling in flexible multibody systems [5, p. 173], Cardona and Géradin address the rolling of the elastic wheel with a slip-stiction approach involving a regularization function proposed by Oden and Martins in [6, p. 587]. The authors describe such function as problematic with regard to the numerical integration when a perfect zero slipping situation is encountered. However, the retained approach is considered for its simplicity compared to schemes involving constraints activation and deactivation which are regarded as complicated in terms of the time integration procedure. As, according to the authors, they cause violent oscillations of constraints and velocities in the transition phases from the sliding to the stiction cases.

Through the relaxation of constraints, we have presented in [2] a simple method for the simulation of a rolling wheel, which amounts to a smooth activation and deactivation of such constraints, without the inconveniences experienced otherwise. The extended Udwadia-Kalaba equations of motion and the N matrix of constraints relaxation we have introduced, both add a new feature to the multibody dynamics formalism. Such a contribution equally applies to the treatment of a variety of multibody systems that involve intermittent constraints. With our approach, a realistic modeling of ground vehicles can be envisioned. Among other applications, thanks to an accurately modeled target vehicle, an improved automated HIL test procedure for different controllers can be achieved, for both performance and safety goals. While the otherwise involved computations are smoothly performed without upsetting the numerical processes. Thanks to the provided explicit form of the equations of motion of an ODE type which, by an appropriate integration scheme, alleviates the burden of DAE integration and does not require to be rewritten either when constraints vanish. To the best of our knowledge [7], under the *Nil novi sub sole* provision, no such developments have been presented prior to this work [2].

 DOI: 10.4236/oalib.1109420

2 The equations of motion of constrained systems and their relaxation

2.1 The Udwadia-Kalaba formulation

Udwadia and Kalaba [4] provide the explicit equations of motion of constrained systems by the following formulation:

$$\begin{cases} M(\boldsymbol{q})\,\ddot{\boldsymbol{q}} = Q + Q^c & \text{(1a)} \\ A\,\ddot{\boldsymbol{q}} = \boldsymbol{b} & \text{(1b)} \end{cases}$$

M is the n-order positive definite mass matrix, and $\boldsymbol{q}$ is the n dimensional generalized coordinates vector. Matrix A with dimension $m \times n$ and m dimensional vector $\boldsymbol{b}$ are obtained from the m constraints functions of m_1 geometric (2a) or m_2 kinematical (2b) kinds.

$$\begin{cases} \boldsymbol{h}_g(\boldsymbol{q}, t) = \boldsymbol{0} & \text{(2a)} \\ \boldsymbol{h}_k(\boldsymbol{q}, \dot{\boldsymbol{q}}, t) = \boldsymbol{0} & \text{(2b)} \end{cases}$$

Constraint matrix A in (1b) is given by:

$$A_{ij} = \begin{cases} \partial h_i/\partial q_j, & i = 1...m_1 \\ \partial h_{i-m_1}/\partial \dot{q}_j, & i = m_1 + 1...m_1 + m_2 \end{cases}, \quad j = 1...n$$

Constraints vector $\boldsymbol{b}$ with dimension $m = m_1 + m_2$ is obtained from (1b) and (3). Q in (1a) is the matrix of generalized applied forces, conservative or dissipative forces and other complementary inertial forces which do not depend on $\ddot{\boldsymbol{q}}$. Q^c represents the reaction forces that are needed to fulfill the constraints. Constraints (2) are differentiated accordingly to get the second derivative:

$$\boldsymbol{0} = \ddot{\boldsymbol{h}}(\ddot{\boldsymbol{q}}, \dot{\boldsymbol{q}}, \boldsymbol{q}, t) = A(\boldsymbol{q}, t)\ddot{\boldsymbol{q}} + \left(\dot{A}(\dot{\boldsymbol{q}}, \boldsymbol{q}, t) + \frac{\partial^2 \boldsymbol{h}(\boldsymbol{q}, t)}{\partial t \partial \boldsymbol{q}} \right) \dot{\boldsymbol{q}} + \frac{\partial^2 \boldsymbol{h}(\boldsymbol{q}, t)}{\partial t^2} \tag{3}$$

According to [8], this differentiation amounts to a DAE index reduction that leads to a mild instability of the manifold (3). The Baumgarte technique [9] which would consider unsatisfied (2a) and (2b) as invariant manifolds on the ODE (1a) aims at rendering manifold (3) attracting. By replacing (3) with:

$$\boldsymbol{0} = \ddot{\boldsymbol{h}} + 2\gamma\dot{\boldsymbol{h}} + \gamma^2\boldsymbol{h}, \quad \text{with} \quad \gamma \geq 0 \tag{4}$$

Where $\gamma = 0$ corresponds to a mildly unstable problem with linearly growing perturbations. Whereas $\gamma > 0$ would cause such perturbations to decrease with time. Analytically, the greater the value of γ, the more attracting the manifold, i.e, asymptotically stable. However, a unanimous grief expressed against Baumgarte is that this property is not verified numerically. But, in the context of this work, the ODE in the UK formulation with the Baumegarte invariants is shown to be part of a stabilization scheme detailed in [10] that effectively addresses this shortcoming for multibody problems with nonholonomic constraints.

 DOI: 10.4236/oalib.1109420

2.2 Relaxation of the constrained equations

The Gauss least-constraint principle [11] states that the actual motion of a constrained system is the one that minimizes the function:

$$G = (\ddot{\boldsymbol{q}} - \boldsymbol{a})^T M(\ddot{\boldsymbol{q}} - \boldsymbol{a}) \tag{5}$$

subject to some constraints $\boldsymbol{h}(\boldsymbol{q}, \dot{\boldsymbol{q}}, t) = \boldsymbol{0}$. Which after an appropriate number of time differentiations generally result in a linear form identical to (1b). The least-constraint principle clearly amounts to a least-square problem (1b) for a weighted minimum-norm solution $\|\ddot{\boldsymbol{q}}\|_M$ from (5). Building on Gauss' least-constraint principle, in order to obtain the Udwadia-Kalaba explicit form of the equations of motion [4] subject to the constraints (1b), we set $\ddot{\boldsymbol{q}} = \boldsymbol{d} + \boldsymbol{a}$. Constraints (1b) can then be written as

$$A(\boldsymbol{d} + \boldsymbol{a}) = \boldsymbol{b} \Leftrightarrow A\boldsymbol{d} = \boldsymbol{b} - A\boldsymbol{a} \Rightarrow \boldsymbol{d} = X(\boldsymbol{b} - A\boldsymbol{a}) + (I - XA)\,\boldsymbol{z} \tag{6}$$

Since $\ddot{\boldsymbol{q}} = \boldsymbol{d}+\boldsymbol{a}$ in (6), we have $M\ddot{\boldsymbol{q}} = M(\boldsymbol{d}+\boldsymbol{a}) = M\boldsymbol{a}+M\boldsymbol{d}$. Knowing that $\boldsymbol{a} = M^{-1}Q$, we obtain:

$$M\ddot{\boldsymbol{q}} = Q + MX(\boldsymbol{b} - A\,\boldsymbol{a}) + M(I - XA)\boldsymbol{z} \tag{7}$$

Noting by (6) that $\boldsymbol{z}$ is an acceleration, it can conveniently be represented by $M^{-1}C$. Where C is a n dimensional force vector which describes the non-ideal contribution. The constraints are readily obtained in an explicit form in (8a), for the ideal contribution, and (8b) for the non-ideal contribution.

$$Q_i^c = MX(\boldsymbol{b} - A\,\boldsymbol{a}) \tag{8a}$$

$$Q_{ni}^c = M(I - XA)M^{-1}C \tag{8b}$$

For the constraints relaxation problem, we suggested in [2] X in the following form:

$$X = M^{-\frac{1}{2}} \left(\left(N^{\frac{1}{2}} \right)^+ AM^{-\frac{1}{2}} \right)^+ N^{\frac{1}{2}}, \quad N = diag(s_i^2) \quad \text{with} \quad i = 1..m \tag{9}$$

Where N represents the m order positive semidefinite relaxation matrix with weights $0 \leqslant s_i \leqslant 1$.

The relaxation of constraints (1b) can be achieved otherwise by considering the more general problem (10) with constraints (10b):

$$\begin{cases} M(\boldsymbol{q})\,\ddot{\boldsymbol{q}} = Q + Q^c & \text{(10a)} \\ NA\,\ddot{\boldsymbol{q}} = N\boldsymbol{b} & \text{(10b)} \end{cases}$$

The constraints forces (8) are reformulated as follows:

$$Q_i^c = MY(N\boldsymbol{b} - NA\,\boldsymbol{a}) \tag{11a}$$

$$Q_{ni}^c = M(I - YNA)M^{-1}C \tag{11b}$$

 DOI: 10.4236/oalib.1109420

With

$$Y = XN^{+} = M^{-\frac{1}{2}}\left(\left(N^{\frac{1}{2}}\right)^{+} AM^{-\frac{1}{2}}\right)^{+}\left(N^{\frac{1}{2}}\right)^{+} \tag{12}$$

Where we used the fact that $N^{1/2}N^{+} = N^{1/2}(N^{1/2})^{+}(N^{1/2})^{+} = (N^{1/2})^{+}$, by virtue of the reverse law applied to generalized inverses for the product of a matrix with its transpose. Matrix Y has the following properties:

$$NAYA = NA \quad MYAY = MY \quad (AY)^{T}N = NAY \quad (YA)^{T}M = MYA \tag{13}$$

For $r(A^{T}NA) = r(A)$, (13) is necessary and sufficient for Y to be A_{NM}[12]. With $\{A_{NM}\}$ being the class of matrices G such that $\hat{\boldsymbol{x}} = G\boldsymbol{y}$ is a minimum M-seminorm among the N-semi-least squares solutions of the possibly inconsistent system $A\boldsymbol{x} = \boldsymbol{y}$. In other words, $\hat{\boldsymbol{x}}$ minimizes $(\boldsymbol{y} - A\boldsymbol{x})^{T}N(\boldsymbol{y} - A\boldsymbol{x})$ or $(N^{1/2}\boldsymbol{y} - N^{1/2}A\boldsymbol{x})^{T}(N^{1/2}\boldsymbol{y} - N^{1/2}A\boldsymbol{x})$. Also, $\hat{\boldsymbol{x}} = G\boldsymbol{y}$ is such that $\|\boldsymbol{y} - AG\boldsymbol{y}\|_{N} \leqslant \|\boldsymbol{y} - A\boldsymbol{x}\|_{N}$. This establishes the link with the projection $P_{A(N)} = AG$ of $\boldsymbol{y}$ onto $\mathcal{R}(A)$ with respect to $\|\boldsymbol{y}\|_{N} = (\boldsymbol{y}^{T}N\boldsymbol{y})^{\frac{1}{2}}$. As $\|\boldsymbol{y} - P_{A}\boldsymbol{y}\|_{N} \leqslant \|\boldsymbol{y} - A\boldsymbol{x}\|_{N}$. Or $\|N^{1/2}\boldsymbol{y} - N^{1/2}P_{A(N)}\boldsymbol{y}\|_{2} = \|N^{1/2}\boldsymbol{y} - P_{NA(I)}N^{1/2}\boldsymbol{y}\|_{2} \leqslant \|N^{1/2}\boldsymbol{y} - N^{1/2}A\boldsymbol{x}\|_{2}$, $\forall \boldsymbol{x} \in \mathbb{R}^{n}, \forall \boldsymbol{y} \in \mathbb{R}^{m}$, for the system $NA\boldsymbol{x} = N\boldsymbol{y}$. Knowing that $N^{1/2}P_{A(N)} = P_{NA(I)}N^{1/2}$ according to [12]. When N is positive definite, A_{NM} is the weighted Moore-Penrose inverse

$$Y = M^{-\frac{1}{2}}\left(N^{\frac{1}{2}}AM^{-\frac{1}{2}}\right)^{+}N^{\frac{1}{2}} \tag{14}$$

which uniquely verifies the four Moore-Penrose conditions:

$$AYA = A, \quad YAY = A, \quad (NAY)^{T} = NAY, \quad (MYA)^{T} = MYA \tag{15}$$

Provided $r(NA) = r(N)$ [13] , the constraints (10b) are consistent. Indeed, it can readily be seen that $NA\boldsymbol{x} \in \mathcal{R}(NA)$. And $N\boldsymbol{b} \in \mathcal{R}(N) = \mathcal{R}(NA)$, because $\mathcal{R}(NA) \subseteq \mathcal{R}(N)$ is always true and equality is met when $dim(\mathcal{R}(NA)) = dim(\mathcal{R}(N))$, meaning $r(NA) = r(N)$. Which is assumed here. Consistency is thus established under the provided condition. And because in the context of this work, $A \in \mathbb{R}_{r}^{m\times n}$, and $N \in \mathbb{R}_{s}^{m\times m}$, where $0 < s \leqslant r$, with N diagonal and positive semidefinite, we do have $r(NA) = r(N)$ fulfilled. With (10b) consistent, Y provides the M-minimum norm solution among all the solutions that actually verify (10b), not in the least-square sense. Y is only required to be an $\{1, 4M\}$ inverse for which:

$$AYA = A, \quad (MYA)^{T} = MYA \tag{16}$$

Hence, the generalized inverse in (14) would have a simpler expression:

$$Y = M^{-\frac{1}{2}}\left(AM^{-\frac{1}{2}}\right)^{+} \tag{17}$$

Compared with the suggested weighted Moore-Penrose inverses (14) and (17), which are based on assumptions that might well be challenged numerically, it appears (9) has the advantage of encompassing all the situations where N is only required to be positive semidefinite, with possibly inconsistent constraints.

 DOI: 10.4236/oalib.1109420

2.3 Stabilization of the equations of motion

For the stabilization examination, as a nominal system, we will first consider a system with ideal constraints, with M positive definite and N nonnegative definite. The UK equations can be rephrased in the following state-space form:

$$\begin{cases} \dot{\tilde{\boldsymbol{q}}} = \tilde{\boldsymbol{v}} & \text{(18a)} \\ \dot{\tilde{\boldsymbol{v}}} = \tilde{\boldsymbol{a}} + \tilde{Y}(\tilde{\boldsymbol{b}} - \tilde{A}\tilde{\boldsymbol{a}}) = \tilde{\boldsymbol{a}} + \tilde{Y}\left(-\dfrac{\partial \tilde{A}\tilde{\boldsymbol{v}}}{\partial \tilde{\boldsymbol{q}}}\tilde{\boldsymbol{v}} - \tilde{A}\tilde{\boldsymbol{a}}\right) & \text{(18b)} \end{cases}$$

Where we have set $\tilde{\boldsymbol{x}} = M^{1/2}\boldsymbol{x}$, $\tilde{\boldsymbol{y}} = \left(N^{1/2}\right)^{+}\boldsymbol{y}$, $\forall \boldsymbol{x} \in \mathbb{R}^n, \boldsymbol{y} \in \mathbb{R}^m$. And $\tilde{A} = \left(N^{1/2}\right)^{+} AM^{-1/2}$, also $\tilde{Y} = M^{1/2}Y\left(N^{1/2}\right)^{+}$. For Y given by (12). By writing

$$\boldsymbol{z} = \begin{bmatrix} \tilde{\boldsymbol{q}} \\ \tilde{\boldsymbol{v}} \end{bmatrix}, \quad \hat{\boldsymbol{h}}(\boldsymbol{z}) = \begin{bmatrix} \tilde{\boldsymbol{g}}(\tilde{\boldsymbol{q}}) \\ \tilde{A}(\tilde{\boldsymbol{q}})\tilde{\boldsymbol{v}} \end{bmatrix}, \quad H = \hat{\boldsymbol{h}}_z \begin{bmatrix} \tilde{A} & 0 \\ \frac{\partial \tilde{A}\tilde{\boldsymbol{v}}}{\partial \tilde{\boldsymbol{q}}} & \tilde{A} \end{bmatrix} \tag{19}$$

(18) is stabilized according to [10] by the following scheme

$$\dot{\boldsymbol{z}} = \hat{\boldsymbol{f}} - \gamma F(\boldsymbol{z})\,\hat{\boldsymbol{h}}(\boldsymbol{z}) \tag{20}$$

Which has the same solution as (18) on the manifold $\mathcal{M} \equiv \hat{\boldsymbol{h}}(\boldsymbol{z}) = \boldsymbol{0}$. Stability [14] is achieved by considering the Lyapunov function $V = \frac{1}{2}\hat{\boldsymbol{h}}^T\hat{\boldsymbol{h}}$, and its derivative:

$$\dot{V} = \hat{\boldsymbol{h}}^T\dot{\hat{\boldsymbol{h}}} = \hat{\boldsymbol{h}}^T H\dot{\boldsymbol{z}} = \hat{\boldsymbol{h}}^T H(\hat{\boldsymbol{f}} - \gamma F\hat{\boldsymbol{h}}) \tag{21}$$

By choosing F such that HF is symmetric positive semidefinite with λ_0 as the largest eigenvalue and by determining γ_0 such that $\|H\hat{\boldsymbol{f}}(\boldsymbol{z})\| \leqslant \gamma_0\|\hat{\boldsymbol{h}}(\boldsymbol{z})\|$, $\forall \boldsymbol{z}$ near $\mathcal{M} \equiv \hat{\boldsymbol{h}}(\boldsymbol{z}) = \boldsymbol{0}$, exponential stability is found for $\gamma > \gamma_0/\lambda_0$ as $\dot{V} \leqslant (\gamma_0 - \gamma\,\lambda_0)\hat{\boldsymbol{h}}^T\hat{\boldsymbol{h}} < 0$. For multibody systems with nonholonomic constraints, we would have (19) as

$$\hat{\boldsymbol{h}}(\boldsymbol{z}) = \begin{bmatrix} 0 \\ \tilde{A}\tilde{\boldsymbol{v}} \end{bmatrix}, \quad H\hat{\boldsymbol{f}} = \begin{bmatrix} 0 \\ -\tilde{\boldsymbol{b}} + \tilde{A}\tilde{\boldsymbol{a}} + \tilde{A}\tilde{Y}(\tilde{\boldsymbol{b}} - \tilde{A}\tilde{\boldsymbol{a}}) \end{bmatrix} = \begin{bmatrix} 0 \\ \tilde{\boldsymbol{c}} \end{bmatrix} \tag{22}$$

After development, it can be seen that $\tilde{\boldsymbol{c}} = \left(I - P_{NA(I)}\right)\left(N^{1/2}\right)^{+}(A\boldsymbol{a} - \boldsymbol{b})$. Where $P_{NA(I)} = \left(\left(N^{1/2}\right)^{+} AM^{-1/2}\right)\left(\left(N^{1/2}\right)^{+} AM^{-1/2}\right)^{+}$. This implies

$$\left\|H\hat{\boldsymbol{f}}\right\| \leqslant \left\|\left(N^{1/2}\right)^{+}(A\boldsymbol{a} - \boldsymbol{b})\right\| \leqslant \lambda_{max}\left(\left(N^{1/2}\right)^{+}\right)\left\|\hat{\boldsymbol{h}}\right\| = \gamma_0\left\|\hat{\boldsymbol{h}}\right\|$$

By choosing,

$$F = \begin{bmatrix} 0 \\ \tilde{Y} \end{bmatrix}, \quad \text{so that,} \quad HF = \begin{bmatrix} \tilde{A} & 0 \\ \frac{\partial \tilde{A}\tilde{\boldsymbol{v}}}{\partial \tilde{\boldsymbol{q}}} & \tilde{A} \end{bmatrix}\begin{bmatrix} 0 \\ \tilde{Y} \end{bmatrix} = \begin{bmatrix} 0 \\ \tilde{A}\tilde{Y} \end{bmatrix} = \begin{bmatrix} 0 \\ P_{NA(I)} \end{bmatrix},$$

as $P_{NA(I)}$ is such that $P_{NA(I)} = B = B^2 = B^TB$ is symmetric and positive semidefinite by definition, exponential stability is established in the sense of Lyapunov for $\gamma > \gamma_0/\lambda_0$. Baumegarte stabilization is verified by observing that $\dot{\boldsymbol{z}} = \hat{\boldsymbol{f}} - \gamma F(\boldsymbol{z})\,\hat{\boldsymbol{h}}(\boldsymbol{z}) = \hat{\boldsymbol{f}} - \gamma\tilde{Y}(\boldsymbol{z})\,\hat{\boldsymbol{h}}(\boldsymbol{z})$. Which amounts to simply incorporating the stabilizing term $-\gamma\dot{\hat{\boldsymbol{h}}}$ into the acceleration compensation factor $(\tilde{\boldsymbol{b}} - \tilde{A}\tilde{\boldsymbol{a}})$ in the extended Udwadia-Kalaba fundamental equation(18b).

 DOI: 10.4236/oalib.1109420

The impact of the non-ideal constraints term on stability will be dealt with as a disturbance to the nominal system. For an exponentially stable nominal system,

$$\dot{\boldsymbol{z}} = \boldsymbol{f}_n(\boldsymbol{z}) \quad \text{where} \quad \boldsymbol{f}_n = \hat{\boldsymbol{f}} - \gamma F(\boldsymbol{z})\hat{\boldsymbol{h}}(\boldsymbol{z}), \tag{23}$$

with the invariant manifold $\mathcal{M} \equiv \hat{\boldsymbol{h}}(\boldsymbol{z}) = \boldsymbol{0}$ assimilated to an equilibrium state solution of an ODE , stability of a disturbed system,

$$\dot{\boldsymbol{z}} = \boldsymbol{f}_n(\boldsymbol{z}) + \boldsymbol{g}(t, \boldsymbol{z}), \tag{24}$$

with $\boldsymbol{g}(t, \boldsymbol{z})$ as the disturbing term, is examined here [15] by considering the Lyapunov function $V(\hat{\boldsymbol{h}})$ of the nominal system as a candidate in order to verify whether the manifold $\mathcal{M} \equiv \hat{\boldsymbol{h}}(\boldsymbol{z}) = \boldsymbol{0}$ is an equally stable invariant set for the disturbed system. Stability of the manifod $\mathcal{M}$ is achieved when, for each $\epsilon > 0$, there is a $\delta(\epsilon, t_0) > 0$ such that

$$d(\boldsymbol{z}(0), \mathcal{M}) < \delta \Rightarrow d(\boldsymbol{z}(t), \mathcal{M}) < \epsilon, \quad \forall t > t_0$$

Because $\dot{V} \leq (\gamma_0 - \gamma\lambda_0)\hat{\boldsymbol{h}}^T\hat{\boldsymbol{h}} = -\lambda V$, the nominal system is exponentially stable with $\hat{\boldsymbol{h}}(\boldsymbol{z}) = \boldsymbol{0}$ as a stable invariant set. It is readily seen that $V(\hat{\boldsymbol{h}}) = \frac{1}{2}\hat{\boldsymbol{h}}^T\hat{\boldsymbol{h}}$ satisfies [15, p. 92]

$$\sigma_1\|\hat{\boldsymbol{h}}\|^2 \leq V(\hat{\boldsymbol{h}}) \leq \sigma_2\|\hat{\boldsymbol{h}}\|^2, \quad \frac{\partial V}{\partial \hat{\boldsymbol{h}}}\boldsymbol{f}_n(\boldsymbol{z}) \leq -\sigma_3\|\hat{\boldsymbol{h}}\|^2, \quad \left\|\frac{\partial V}{\partial \hat{\boldsymbol{h}}}\right\| \leq \sigma_4\|\hat{\boldsymbol{h}}\|$$

Assuming that the perturbation function $\boldsymbol{g}(t, \boldsymbol{z})$ has a bound such that

$$\|\boldsymbol{g}(t, \boldsymbol{z})\| \leq \alpha\|\hat{\boldsymbol{h}}\|, \quad \forall t \geq 0, \quad \text{with} \quad \alpha \geq 0,$$

from $\dot{V}(t, \hat{\boldsymbol{h}}) = \frac{\partial V(\hat{\boldsymbol{h}})}{\partial \hat{\boldsymbol{h}}}\boldsymbol{f}_n(\boldsymbol{z}) + \frac{\partial V(\hat{\boldsymbol{h}})}{\partial \hat{\boldsymbol{h}}}\boldsymbol{g}(t, \boldsymbol{z})$, we have

$$\dot{V}(t, \hat{\boldsymbol{h}}) \leq -\sigma_3\|\hat{\boldsymbol{h}}\|^2 + \left\|\frac{\partial V}{\partial \hat{\boldsymbol{h}}}\right\| \|\boldsymbol{g}(t, \boldsymbol{z})\| \leq -\sigma_3\|\hat{\boldsymbol{h}}\|^2 + \sigma_4\alpha\|\hat{\boldsymbol{h}}\|^2$$

Provided $\alpha < \frac{\sigma_3}{\sigma_4}$, $\dot{V}(t, \hat{\boldsymbol{h}}) \leq -(\sigma_3 - \sigma_4\alpha)\|\hat{\boldsymbol{h}}\|^2$ would conclusively establish the manifold $\mathcal{M} \equiv \hat{\boldsymbol{h}}(\boldsymbol{z}) = \boldsymbol{0}$ as an exponentially stable invariant set according to Khalil approach in [15].

In the context of the problem we are concerned with, we observe that for

$$\boldsymbol{g}(t, \boldsymbol{z}) = (I - YNA)M^{-1}C$$

we have $\|(I - YNA)M^{-1}C\| < \|M^{-1}C\|$, by virtue of the fact that $\boldsymbol{g}(t, \boldsymbol{z})$ constitutes the projection of $M^{-1}C$ on the null space of NA. Since $M > 0$, we also have $\|M^{-1}C\| \leq \lambda_{max}\left(M^{-1}\right)\|C\|$.

By determining $C_i = \mu N_{ci} \tanh\left(\frac{\tau_i}{\mu N_{ci} R}\right) \tanh(\hat{h}_i)$ so that $|C_i| \leq \mu N_{ci} |\tanh(\hat{h}_i)| \leq \Gamma_i|\hat{h}_i|$, with $\Gamma_i = \mu N_{ci}$, we finally verify that

$$\|\boldsymbol{g}(t, \boldsymbol{z})\| \leq \frac{1}{\lambda_{min}(M)}\|\Gamma\|\|\hat{\boldsymbol{h}}\| = \alpha\|\hat{\boldsymbol{h}}\|$$

which qualifies the constraints $\hat{\boldsymbol{h}} = \boldsymbol{0}$ as an exponentially stable invariant set for the disturbed problem with the non-ideal constraints force.

 DOI: 10.4236/oalib.1109420

3 The half car model

3.1 Problem description

A half-car model is represented in Fig. 15. The car is to be moved on an occasionally slippery road. A torque is applied progressively on the rear wheel. The front wheel is free to roll. We would like to determine the dynamics of both wheels with respect to the stiction and slip phases.

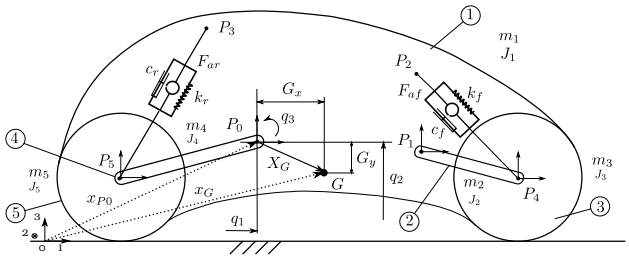

Figure 1: Chassis parameters.

3.2 The multibody system

Relative coordinates are used to position the parts. Body 1 is the chassis with three generalized coordinates q_1, q_2, q_3. It is characterized by mass m_1 and inertia J_1. Points P_0, P_1, P_2, and P_3 are attached to the chassis. Body 2 and 3 are respectively the front arm and the front wheel as shown in Fig. 2. The former is positioned with relative generalized coordinate q_4, the later with q_5. Body 2 is characterized by mass m_2, inertia J_2 and length L_2. It bears attachment point P_4. Body 3 shows mass m_3, inertia J_3, stiffness k_{fw}, damping c_{fw}, and undeformed radius r_{fw0}.

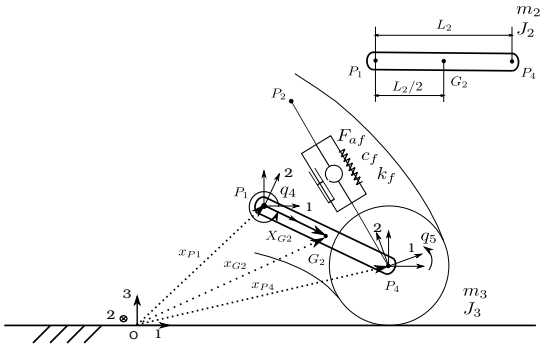

Figure 2: Car front arm and wheel parameters.

 DOI: 10.4236/oalib.1109420

Similarly, body 4 and 5 in Fig. 3 are respectively the rear arm and wheel. Body 4 with attachment point P_5 is positioned by coordinate q_7 while q_6 positions body 5. The system has 7 degrees of freedom in an open-tree configuration.

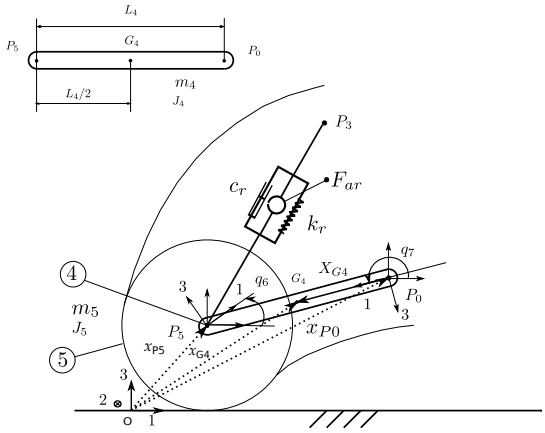

Figure 3: Car rear arm and wheel parameters.

In [5], Cardona and Géradin present both the rigid and the flexible body dynamics for the generation of the equations of motion of a multibody system. Figure 4 shows a rigid body. The position $\boldsymbol{x}_P$ of a given point P on a body in the reference frame is expressed here as:

$$\boldsymbol{x}_P = \boldsymbol{x}_o + R\boldsymbol{X} \tag{25}$$

$\boldsymbol{X}$ is the vector of the same point P on the body in the local frame. R is the rotation matrix which lines are orthogonal projections of the reference frame base vectors onto the local frame. For rigid bodies in which $\dot{\boldsymbol{X}} = \boldsymbol{0}$, (25) implies

$$\dot{\boldsymbol{x}}_P = \dot{\boldsymbol{x}}_o + \dot{R}\boldsymbol{X} + R\dot{\boldsymbol{X}} = \dot{\boldsymbol{x}}_o + \dot{R}R^T\boldsymbol{x} = \dot{\boldsymbol{x}}_o + \tilde{\omega}\boldsymbol{x} = \dot{\boldsymbol{x}}_o + \tilde{\omega}(\boldsymbol{x}_P - \boldsymbol{x}_o) \tag{26}$$

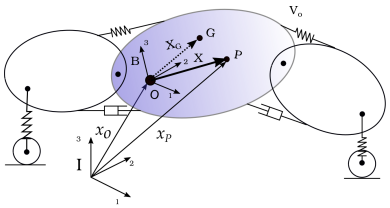

Figure 4: Body with point P in local frame vs reference frame.

Which in the local frame, by premultiplying (26) by R^T, corresponds to

$$\dot{\boldsymbol{X}} = R^T\dot{\boldsymbol{x}}_o + R^T\dot{R}\boldsymbol{X} = R^T\dot{\boldsymbol{x}}_o + \tilde{\Omega}\boldsymbol{X} = \boldsymbol{0} \quad \text{where} \quad \tilde{\Omega} = R^T\dot{R} \tag{27}$$

 DOI: 10.4236/oalib.1109420

3.3 Constraints equations.

The pure rolling condition is expressed by equating to zero the slipping speed of the wheels. Such a slipping speed is the speed of contact point x_{Ci}^K attached to the road as measured in non-rotating frame of the wheel frame K.

$$\dot{\boldsymbol{x}}_{Ci}^I = \dot{\boldsymbol{x}}_{Oi}^I + \dot{R}R^T \boldsymbol{x}_{Ci}^K = \dot{\boldsymbol{x}}_{Oi} + \tilde{\omega}_i(\boldsymbol{x}_{Ci}^I - \boldsymbol{x}_{Oi}^I) \tag{28}$$

For the rear wheel, $\dot{\boldsymbol{x}}_{Oi} = \dot{\boldsymbol{x}}_{P_5} = \dot{\boldsymbol{x}}_{P_0} + \dot{R}_{ra}\boldsymbol{X}_{P_5}$. With $\boldsymbol{x}_{P5} = \boldsymbol{x}_{P_0} + R_{ra}\boldsymbol{X}_{P_5}$. For the front wheel, $\dot{\boldsymbol{x}}_{Oi} = \dot{\boldsymbol{x}}_{P_4} = \dot{\boldsymbol{x}}_{P_1} + \dot{R}_{fa}\boldsymbol{X}_{P_4}$, with $\dot{\boldsymbol{x}}_{P_1} = \dot{\boldsymbol{x}}_{P_0} + \dot{R}_1\boldsymbol{X}_{P_1}$. And $\boldsymbol{x}_{P4} = \boldsymbol{x}_{P_1} + R_1\boldsymbol{X}_{P_4}$. The constraints equations for both wheels are (28):

$$\begin{cases} \dot{h}(1) \equiv \dot{\boldsymbol{x}}_{P4}(1) - (\dot{q}_3 + \dot{q}_4 + \dot{q}_5)\,\boldsymbol{x}_{P4}(3) = 0 & \text{(29a)} \\ \dot{h}(2) \equiv \dot{\boldsymbol{x}}_{P4}(3) = 0 & \text{(29b)} \\ \dot{h}(3) \equiv \dot{\boldsymbol{x}}_{P5}(1) - (\dot{q}_3 + \dot{q}_6 + \dot{q}_7)\,\boldsymbol{x}_{P5}(3) = 0 & \text{(29c)} \\ \dot{h}(4) \equiv \dot{\boldsymbol{x}}_{P5}(3) = 0 & \text{(29d)} \end{cases}$$

The velocity-based constraints matrix A is obtained by deriving (2b) once with respect to $\dot{\boldsymbol{q}}$.

$$A_{ij} = \frac{\partial \dot{h}_i}{\partial \dot{q}_j} \tag{30}$$

Assuming scleronomic constraints, vector $\boldsymbol{b}$ in the motion equation (1) is then obtained from (3) as follows

$$b_i = -\sum_{j=1}^{n}\sum_{k=1}^{n} \frac{\partial A_{ij}}{\partial q_k}\dot{q}_j\dot{q}_k \tag{31}$$

The constraints-weights matrix N is given by:

$$N = \begin{bmatrix} s_f^2 & 0 & 0 & 0 \\ 0 & s_r^2 & 0 & 0 \\ 0 & 0 & s_f^2 & 0 \\ 0 & 0 & 0 & s_r^2 \end{bmatrix}, \quad s_i = 1 - \tanh^2\left(\tfrac{1}{3}k_s\tfrac{T_{mi}+T_{bi}}{\mu\, N_{ci}\, r_i}\right), \quad i = \{f, r\} \tag{32}$$

The constraints equations in (29) are selectively activated, deactivated or simply discriminated against by the stiction coefficients s_i. Where $i = \{f, r\}$ stand respectively for the front and rear wheel. N_{ci} is the contact reaction force of the ground for each wheel. And $r_r = \boldsymbol{x}_{P5}(3)$ and $r_f = \boldsymbol{x}_{P4}(3)$, the heights of the wheels center. The matrix C of generalized forces for nonideal constraints is

$$C = \begin{bmatrix} F_{ci} & 0 & 0 & 0 & 0 & 0 & 0 \end{bmatrix}^T$$

F_{ci} represents the sliding friction reaction forces on the front and rear wheels.

$$F_{ci} = -\mu N_{ci}\tanh\left(\frac{1}{3}k_F\frac{T_{mi}+T_{bi}}{\mu\, N_{ci}\, r_i}\right)\tanh(\omega_i r_i - \dot{q}_1), \quad i = \{f, r\} \tag{33}$$

 DOI: 10.4236/oalib.1109420

4 Simulations results

A torque T_{mot} is increasingly applied on the rear wheel. The front wheel is free to roll as the vehicle enters a slippery phase. Subsequently, a braking torque is applied on both wheels. The rotational speeds of both wheels are observed. The applied torques are represented in Fig. 5(a) and are given by:

$$T_{mot} = T_{max} \tanh(k_M\, t) \tag{34}$$

, for the driving torque. And the braking torque is

$$T_b = -\frac{T_{bmax}}{4}\left(1 + \frac{1 - e^{-t_{br}(t-t_b)}}{1 + e^{-t_{br}(t-t_b)}}\right)\left(1 + \frac{1 - e^{-t_{br}(t-t_b-b_d)}}{1 + e^{-t_{br}(t-t_b-b_d)}}\right)\tanh(\omega) \tag{35}$$

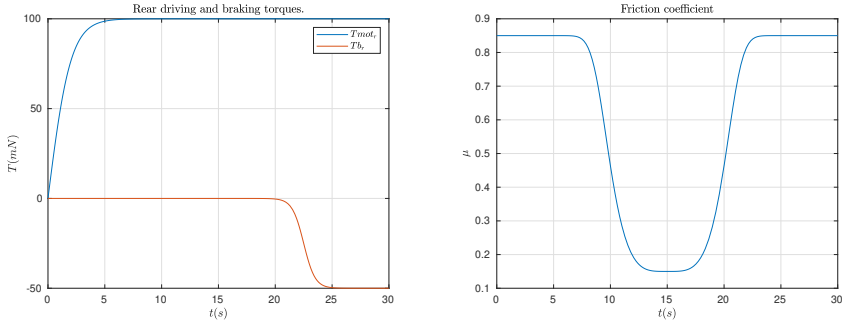

(a) Applied torques. (b) Friction profile.

Figure 5: Simulation input.

The friction coefficient profile, as shown in Fig. 5(b), is

$$\mu(t) = \mu_l + (\mu_u - \mu_l) \cdot \tanh\left(\frac{1}{s_d}(t - t_s)\right)^4 \tag{36}$$

Air resistance is taken into account with the bearing resistance according to:

$$F_w = -\frac{1}{2}\,\rho\, A_r\, c_x\, \dot{q}_1^2, \quad T_{be} = -k_{be}\omega_i^2, \quad i = \{f, r\} \tag{37}$$

For a maximum applied torque of $T_m = 150Nm$, the knematic results of both the rear and the front wheels are shown in Fig. 6. For the rear wheel, a clear increase in speed is observed as the wheel experiences a much lower friction coefficient phase. The traction is displayed in Fig. 8(a). The traction reaction Q_{ci} is saturated by the friction limit μN according to (33). For a higher maximum applied torque $T_{max} = 550\,Nm$, the kinematic results are shown in Fig. 7. A discrepancy is clearly observed in Fig. 7(a) at lower rotational speeds between the rear and the front wheel, though the friction coefficient is relatively high. A greater spinning is observed at a lower friction coefficient value. A distinctly saturated reaction force Q_{ci} is displayed in Fig. 8(b).

 DOI: 10.4236/oalib.1109420

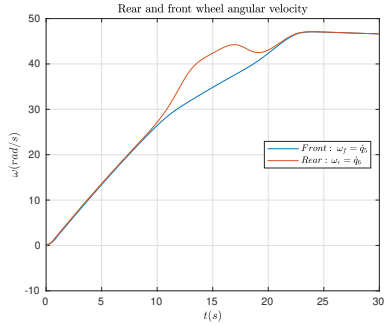

(a) Rotational speeds.

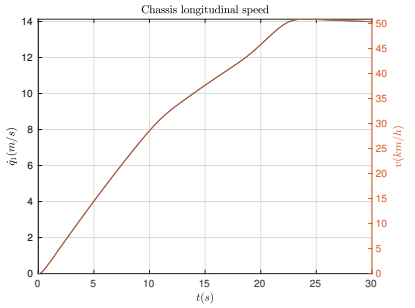

(b) Car speed.

Figure 6: Kinematic results for $T_{max} = 150\,Nm$.

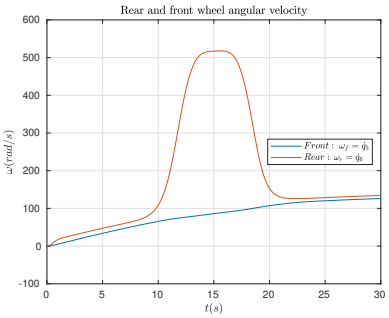

(a) Rotational speeds.

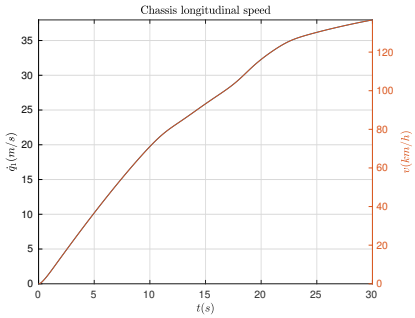

(b) Car speed.

Figure 7: Kinematic results for $T_{max} = 550\,Nm$.

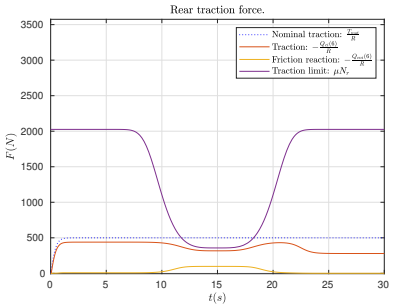

(a) $T_{max} = 150\,Nm$.

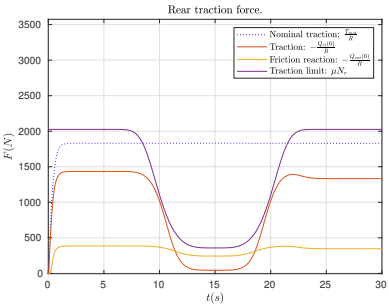

(b) $T_{max} = 550\,Nm$.

Figure 8: Traction Q_i^c and slip Q_{ni}^c reactions on the rear wheel.

The numerical values for the simulation are presented in table 1.

 DOI: 10.4236/oalib.1109420

A much higher torque might be applied to the rear wheel with $T_{max} = 700Nm$. As shown in Fig. 9, the traction reaction force Q_c is saturated to the bottom. The sliding friction reaction is saturated by the friction limit μN.

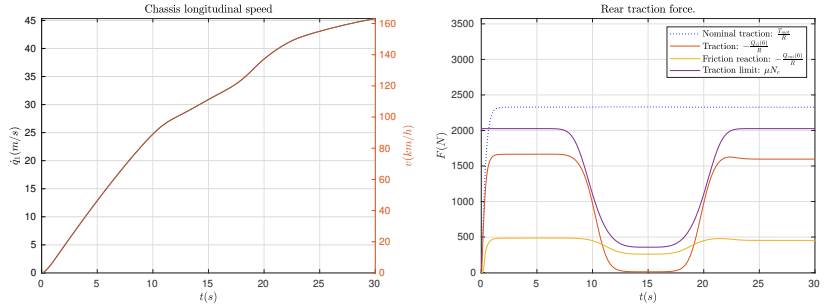

(a) Vehicle speed. (b) Reaction forces with limit.

Figure 9: Simulation results for $T_{max} = 700Nm$.

The front wheel reaction forces of both traction and sliding friction are obtained from the related torques constraint associated with the rotation of the wheel by division by the wheel radius.

Figure 10 shows the existence of a lower tractive reaction on the front that is saturated by the friction limit when an applied torque on the rear wheel has the maximum value of $T_{max} = 150Nm$. Conversely, the friction reaction force is nonexistent since the wheel is rolling freely and is in a stiction mode.

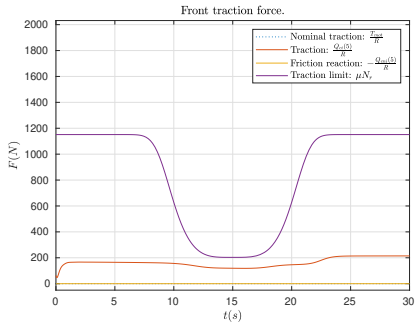

Figure 10: Front wheel reaction forces and limit for $T_{max} = 150Nm$

 DOI: 10.4236/oalib.1109420

Figure 11 shows the traction reaction force on the front which is initially saturated by the friction limit and subsequently goes down as the vehicle is being slowed down by a more accentuated slip created by a higher torque on the rear wheel with $T_{max} = 550Nm$.

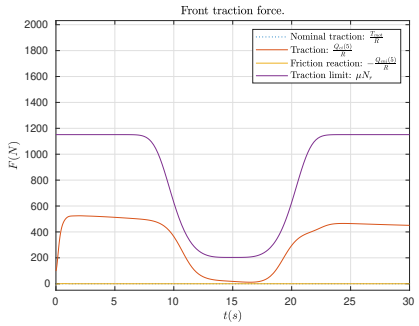

Figure 11: Front wheel reaction forces and limit for $T_{max} = 550Nm$

Figure 12 shows the traction and sliding friction reaction forces on the front wheel for $T_{max} = 700Nm$ on the rear wheel. Interestingly, the traction reaction force on the front is not bounded to zero but displays a negative value.

Contrary to the rear wheel which is under an applied torque of the highest maximum value $T_{max} = 700Nm$ and is mostly in a slip mode, the front wheel remains in stiction mode because there is no applied torque on it. Thus, as the rear traction reaction is zeroed, the wind force F_w takes over the dynamics of the vehicle because of inertia, and slows it down. This is naturally reflected on the front wheel by a braking effort since it is in a stiction mode. Just as any pushing-back force on the vehicle would generate a negative traction force on a free wheel in a stiction mode. Which would cause the braking and ultimately the reversal of its movement. With a null sliding friction reaction force.

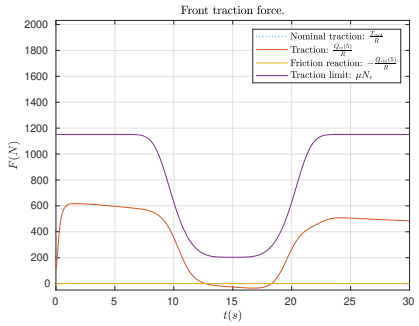

Figure 12: Front wheel reaction forces and limit for $T_{max} = 700Nm$

 DOI: 10.4236/oalib.1109420

4.1 Effect of Baumgarte parameter variation on simulation

Figure 13 shows the effect of increased Baumegarte parameter γ on the rotational speeds of both wheels. The reference case is the one considered in Fig. 7(a) which uses $\gamma = 20$ for a $T_{max} = 550Nm$. Figure 13(b) shows the results for $\gamma = 100$.

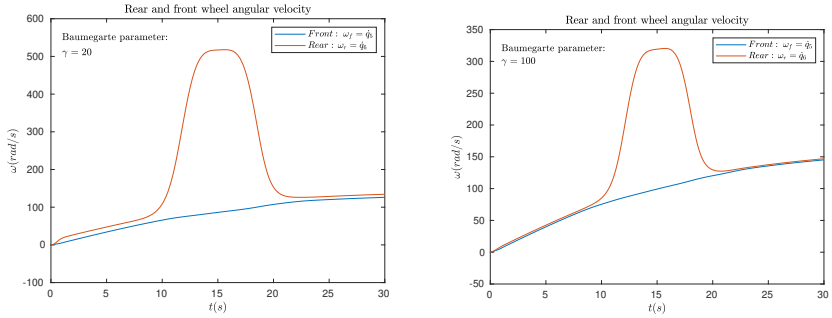

(a) $\gamma = 20$. (b) $\gamma = 100$

Figure 13: Vehicle wheel rotational speeds.

Further increment of Baumegarte parameter to $\gamma = 200$ in Fig. 14(a) and $\gamma = 2000$ as shown in Fig. 14(b) displays the gradually attenuated relaxation of constraints and the accentuated compliance outside the relaxation zone. Which might not be desired as it shadows the effect of higher torques in the relaxation of constraints. However, the attractiveness displayed is indicative of the robustness of the integration scheme with a simple choice of the stabilization parameter that could well be calibrated on experimental results.

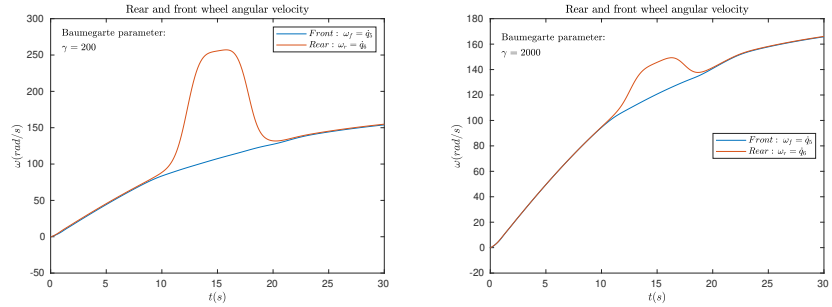

(a) $\gamma = 200$. (b) $\gamma = 2000$

Figure 14: Vehicle wheel rotational speeds.

 DOI: 10.4236/oalib.1109420

Table 1: Numerical values.

Description	**Parameter**	**Value**
Motor		
Torque peak value	T_{max}	$150/550\,Nm$
Torque curve slope	k_M	2
Brake peak value	T_{bmax}	$50\,Nm$
Brake start time	t_b	$3/4\,t_f$
Brake curve slope	T_{br}	2
Brake duration	b_d	t_f
Road		
Friction upper limit	μ_u	0.85
Friction lower limit	μ_l	0.15
Slip duration	s_d	$1/5\,t_f$
Slip start time	t_s	$1/2\,t_f$
Air resistance area	A_r	$2\,m^2$
Air density	ρ	$1.2\,kg/m^3$
Air resistance coefficient	c_x	0.3
Chassis		
Body mass	m_1	$350\,kg$
Body inertia	J_1	$1500\,kg \cdot m^2$
Rear spring stiffness	k_r	$45000\,N/m$
Front spring stiffness	k_f	$40000\,N/m$
Rear damper damping	c_r	$2500\,kg/s$
Front damper damping	c_f	$2500\,kg/s$
$P1$ x coordinate	P_{1X}	$1.2\,m$
$P1$ z coordinate	P_{1Z}	$0.0\,m$
$P2$ x coordinate	P_{2X}	$1.3\,m$
$P2$ z coordinate	P_{2Z}	$0.4\,m$
$P2$ x coordinate	P_{2X}	$1.3\,m$
$P2$ z coordinate	P_{2Z}	$0.4\,m$
$P3$ x coordinate	P_{3X}	$0.4\,m$
$P3$ z coordinate	P_{3Z}	$0.4\,m$
$G1$ x coordinate	G_{1X}	$0.3\,m$
$G1$ z coordinate	G_{1Z}	$0.1\,m$
Rear arm		
Arm mass	m_r	$6\,kg$
Arm length	L_r	$0.5\,m$
Front arm		
Arm mass	m_f	$5\,kg$
Arm length	L_f	$0.5\,m$
Wheels		
Wheel mass	m_w	$10\,kg$
Wheel radius	r_w	$0.25\,m$
Simulation duration	t_f	$30\,s$

 DOI: 10.4236/oalib.1109420

5 Conclusion

In this work, we presented a simple method for the simulation of a rolling wheel for the longitudinal dynamics of a road vehicle.

A new approach for the realistic simulation of the rolling of the elastic wheels is introduced. Such a realistic simulation includes situations such as the spinning of the wheel. Which may originate from the encounter with a lower friction zone or the application of a relatively higher torque with respect to the friction limit. These situations are associated with a breakaway from the constraints equations for pure rolling. To account for such a breakaway, an extended formulation of the Udwadia-Kalaba equations of motion for constrained systems was proposed. The method amounts to a smooth activation and deactivation of constraints that are associated with pure rolling according to the encountered situation of stiction or slip. This is done without the inconveniences experienced otherwise in the referenced literature.

The relaxation of a pure rolling constraint naturally leads to the saturation of the associated constraint force which corresponds to the traction force saturation. Thanks to the extended U-K formulation, the computation of the explicit expression of such a traction force is obtained as a result of the dynamics of the rolling wheel. As opposed to the approach that sets it as an input to the model via some approximate formula.

This in our view opens the path to a whole different philosophy in the design of controllers for wheel slip that a future work will explore. Where slip in itself is not the direct object for control rather the consequence of an appropriately assessed traction reaction effort with regard to the road condition.

Final statement

Funding: This research received no external funding.

Institutional Review Board Statement: Not applicable.

Informed Consent Statement: Not applicable.

Data Availability: The data presented in this study are available on request, from the corresponding author.

Conflict of Interest: The author declares no conflict of interest.

References

[1] Caverley, R., Constrained or unconstrained, that is the equation. *USC News*, September 2001.

[2] Ikoki, B. K., The rolling wheel equations without magic: A combined slip-stiction approach by the Udwadia-Kalaba formulation with constraints relaxation for a smooth simulation. *Journal of Transportation Technologies*, vol. 11, pp. 378–389, June 2021.

[3] Neĭmark, J. I. and Fufaev, N. A., *Dynamics of nonholonomic systems*, vol. 33 of *Translations of mathematical monographs*. AMS, 1972.

[4] Udwadia, F. E. and Kalaba, R., A new perspective on constrained motion. *Proceedings of The Royal Society*, November 1992.

[5] Cardona, A. and Géradin, M., *Flexible multibody dynamics*. Wiley, 2001.

[6] Oden, J. T. and Martins, J., Models and computational methods for dynamic friction phenomena. *Comp. Meth. in Appl. Mech. and Eng.*, vol. 52, pp. 527–634, 1985.

[7] Soltakhanov, S. K., Yushkov, M. P., and Zeghzda, S., *Mechanics of nonholonomic systems*. Springer, 2009.

[8] Ascher, U., Honshen, C., Petzold, L., and Sebastian, R., Stabilization of constrained mechanical systems with DAEs and invariant manifolds. *Mechanics of Structures and Machines*, vol. 23, pp. 135–157, 1995.

[9] Baumgarte, J., Stabilization of constraints and integrals of motion in dynamical systems. *Comp. Math. Appl. Mech. Eng.*, vol. 1, pp. 1–16, June 1972.

[10] Ascher, U. and Chin, H., Stabilization of DAEs and invariant manifolds. *Numerische Mathematik*, vol. 67, pp. 131–149, 03 1994.

[11] Kalaba, R., Natsuyama, H. H., and Udwadia, F. E., An extension of Gauss' principle of least constraint. *International Journal of General Systems*, 2004.

[12] Mitra, S. K. and Rao, C. R., Projections under seminorms and generalized moore penrose inverses. *Linear Algebra and its applications*, vol. 9, 1974.

[13] Stanimirović, P., Pappas, D., Katsikis, V., and Cvetković, M., Outer inverse restricted by a linear system. *Linear and Multilinear Algebra*, vol. 63, pp. 2461–2493, 03 2015.

[14] Lyapunov, A. M., Problème général de la stabilité du mouvement. *Annales de la Faculté des Sciences de Toulouse*, vol. 9, pp. 203–474.

[15] Khalil, K. H., *Nonlinear control*. Pearson Education Limited, 2015.

 DOI: 10.4236/oalib.1109420

Appendices

A Simulation code

The simulation code can be obtained on author's website by scanning the following QR code:

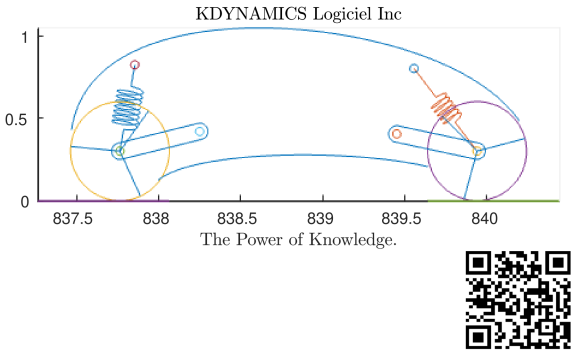

Figure 15: Matlab simulation code address.

 DOI: 10.4236/oalib.1109420